Electromechanical Model of Electrically Actuated Narrow Microbeams

Romesh C. Batra, *ASME, Fellow*, Maurizio Porfiri, and Davide Spinello

***Abstract*—A consistent one-dimensional distributed electromechanical model of an electrically actuated narrow microbeam with width/height between 0.5–2.0 is derived, and the needed pull-in parameters are extracted with different methods. The model accounts for the position-dependent electrostatic loading, the fringing field effects due to both the finite width and the finite thickness of a microbeam, the mid-plane stretching, the mechanical distributed stiffness, and the residual axial load. Both clamped–clamped and clamped-free (cantilever) microbeams are considered. The method of moments is used to estimate the electrostatic load. The resulting nonlinear fourth-order differential equation under appropriate boundary conditions is solved by two methods. Initially, a one-degree-of-freedom model is proposed to find an approximate solution of the problem. Subsequently, the meshless local Petrov–Galerkin (MLPG) and the finite-element (FE) methods are used, and results from the three methods are compared. For the MLPG method, the kinematic boundary conditions are enforced by introducing a set of Lagrange multipliers, and the trial and the test functions are constructed using the generalized moving least-squares approximation. The nonlinear system of algebraic equations arising from the MLPG and the FE methods are solved by using the displacement iteration pull-in extraction (DIPIE) algorithm. Three-dimensional FE simulations of narrow cantilever and clamped–clamped microbeams are also performed with the commercial code ANSYS. Furthermore, computed results are compared with those arising from other distributed models available in the literature, and it is shown that improper fringing fields give inaccurate estimations of the pull-in voltages and of the pull-in deflections. [1641]**

***Index Terms*— Fringing fields, microelectromechanical systems (MEMS), microelectromechanical systems (MEMS) modeling, microactuators, microbeams, microsensors, microstructures, meshless local Petrov–Galerkin (MLPG) method, pull-in instability, pull-in voltage, reduced order models.**

I. Introduction

RECENT technological developments have opened promising research opportunities and engineering priorities in micromechanics. The study of electrostatically actuated microelectromechanical systems (MEMS) is a branch of micromechanics. These MEMS find wide applications in switches [1], micro-mirrors [2], and micro-resonators [3]. At the microscopic scale, high energy densities and large forces are available, and the electrostatic actuation may be more effective than other kinds of actuation.

An electrostatically actuated microbeam is an elastic beam suspended above a stationary rigid plate, both made of conductive materials, and a dielectric medium filling the gap between them. An applied electric voltage between the two electrodes results in the deflection of the elastic beam and a consequent change in the MEMS capacitance. The applied electrostatic force has an upper limit beyond which the electrostatic Coulomb force is not balanced by the elastic restoring force in the deformable beam, the beam spontaneously deflects towards the stationary rigid plate, and the device collapses. This phenomenon, called pull-in instability, was simultaneously observed experimentally in [4] and [5]. The accurate estimation of the pull-in voltage is crucial in the design of electrostatically actuated MEM devices. In particular, in micro-mirrors [2] and micro-resonators [3], the designer avoids this instability in order to achieve stable motions; in switching applications [1], the designer exploits this effect to optimize the device's performance.

Accurate estimates of the pull-in parameters have been obtained by three-dimensional (3-D) numerical simulations based on either the finite-element (FE) or the boundary element analyses (see, e.g., [6] and [7]); however, these approaches are time-consuming. Therefore, considerable effort has been devoted to developing reliable one-dimensional (1-D) distributed models of electrostatically actuated microbeams. In [3], a wide clamped–clamped microbeam is modeled with the classical linear beam theory, and the electrostatic force is computed by completely discarding fringing field effects. These assumptions are justified for small beam deflections and wide beams. In [8], an effective Young's modulus is considered in order to account for plane stress and plane strain deformations appropriate for narrow and wide beams, respectively. The effects of fringing field is considered by accounting for the microbeams' finite width but neglecting their finite thickness. In [9], the beam mid-plane stretching is accounted for in order to treat large deflections. Nevertheless, no improvements with respect to [3] on the electric modeling are shown, rendering this model suitable for wide microbeams with initial gap sizes comparable with the beam thickness. In [10], the fringing field correction of [8] is combined with the finite deflection approach of [9], resulting in a model that accurately predicts the pull-in parameters of wide beams undergoing moderate displacements. None of these works is applicable to narrow beams where effects of fringing fields due to the finite thickness are not negligible, as observed in [11].

Furthermore, the consideration of the mid-plane stretching makes the governing equation nonlinear, and the problem of numerically extracting the pull-in parameters more challenging.

Manuscript received June 28, 2005; revised December 19, 2005. Subject Editor N. Aluru.

M. Porfiri is with the Department of Mechanical, Aerospace and Manufacturing Engineering, Polytechnic University, Brooklyn, NY 11201 USA (e-mail mporfiri@poly.edu).

R. C. Batra and D. Spinello are with the Department of Engineering Science and Mechanics, Virginia Polytechnic Institute and State University, Blacksburg, VA 24061 USA (e-mail: rbatra@vt.edu; dspinell@vt.edu).

Digital Object Identifier 10.1109/JMEMS.2006.880204

The shooting method used in [9] to solve nonlinear differential equations relies on good initial estimates of unknown parameters and may diverge. In [12], two variants of the Galerkin method are employed by using the beam mode shapes as basis functions. In the first variant, the electrostatic force is expanded in Taylor series around the undeformed configuration, and terms up to the fifth order are retained. The second variant accounts exactly for the electrostatic force. The estimate of the pull-in parameter computed with the first method does not agree well with that obtained with the shooting method. The pull-in parameter obtained from the second variant is very sensitive to the number of modes used as basis, and acceptable results are obtained only when an odd number of modes greater than one are included in the basis functions. Both techniques neglect fringing field effects. The use of mode shapes as a basis limits the applicability of the method to beam geometries for which eigenvalues and eigenfunctions can be easily computed. In [10], the differential quadrature method is used and computed results seem very accurate; nevertheless, the global nature of the method seems to forbid its application to more complicated MEMS geometries.

Recently, considerable research in computational mechanics has been devoted to the development of meshless methods; see, e.g., [13] and [14]. These methods are especially useful in problems with discontinuities or moving boundaries, i.e., problems involving large deformations, crack propagation, and high gradients, among others. Meshless methods may also alleviate some other problems associated with the FE method, such as locking and element distortion. In most applications, fewer nodes are needed in the meshless method than those with the FE method to obtain approximate solutions with the same accuracy. Here, we adopt the meshless local Petrov–Galerkin (MLPG) method that has been successfully applied to the analysis of static linear beam and plate problems in [15]–[20]. The MLPG method used here employs the generalized moving least-square (GMLS) basis functions for representing the test and the trial functions. Results are also computed with a 1-D FE code employing Hermitian basis functions (i.e., beam elements) and compared with those obtained from the MLPG method.

In this paper, we present a model for analyzing narrow microbeams undergoing finite deflections. The beam is modeled by using a large deflection theory; see, e.g., [22]. This model does not account for finite deformations and is applicable when the MEMS gap size and the microbeam thickness are considerably smaller than the beam span. Indeed, small strains are experienced whenever the microbeam deflection is much smaller than the microbeam length, even if the maximum deflection exceeds the beam thickness. We solve the resulting nonlinear fourth-order differential equation by using two distinct approaches: 1) reducing the distributed system to a one-degree-of-freedom (1-DOF) system and 2) retaining the distributed system and using the MLPG and the FE methods in conjunction with the efficient displacement iteration pull-in extraction (DIPIE) algorithm developed in [23]. In particular, we derive a consistent electromechanical model where finite thickness of the beam is considered in both the mechanical and the electrical models. With the Method of Moments (MoM) (see, e.g., [24]), an expression for the electrostatic load is established which simultaneously accounts for the fringing field capacitance due to finite width and finite thickness of the microbeam. The approach followed here is similar to that used in structural mechanics to study Saint–Venant problems; see, e.g., [25], that is, deformations of a slender beam are studied by initially solving a two-dimensional (2-D) problem defined on the cross section of the beam and using these results to build a 1-D model of the beam with distributed forces/loads acting on its length. Whereas in [6] a reduced order discrete model valid for a specific MEMS is deduced from 3-D numerical simulations, here a 1-D distributed model of a narrow microbeam is proposed with 2-D numerical simulations needed to determine an expression for the electrostatic force. The present reduced order 1-DOF model differs from the classical mass-spring model of [5], since we account for the axial stress, nonlinear stiffening, charge redistribution, and fringing fields. It also differs from that of [12] since we retain the complete nonlinear behavior of the electrostatic force and consider fringing fields, and it differs from that of [11] since we simultaneously treat the pull-in voltage and deflections as unknowns, i.e., the pull-in deflection is not empirically chosen as was done in [11]. Two sample problems, namely, a cantilever and a clamped–clamped microbeam, are considered. Results from the proposed 1-DOF and the distributed models are compared with those available in the literature [8]–[10] and with those obtained from 3-D FE simulations. Some of the 3-D FE results for a cantilever beam are borrowed from [11]. Other results for the cantilever beam, and results for the clamped–clamped microbeam, have been obtained by using the commercial FE code ANSYS.

Three goals of this paper are: 1) propose a consistent 1-D distributed electromechanical model for a narrow microbeam; 2) establish a reduced-order 1-DOF model that gives a good estimate of the pull-in parameters (deflection and voltage); and 3) extend the MLPG method employed earlier to analyze linear beam problems to the analysis of those nonlinear beam problems where nonlinearities arise simultaneously due to electrostatic loads and membrane stretching.

The remainder of this paper is organized as follows. In Section II, we give governing equations of an electrostatically actuated clamped–clamped and a cantilever narrow microbeam; in Section III, we derive an expression for the distributed electrostatic force that simulates well the fringing field effects. In Section IV, we describe a 1-DOF model, and, in Section V, we briefly present the MLPG and the FE methods and apply the DIPIE algorithm for extracting the pull-in parameters. In Section VI, we compare the proposed fringing fields corrections with some of the classical formulas available in the literature. The proposed 1-DOF and the distributed electromechanical models are validated by comparing their predictions with those from other distributed models and from ANSYS and COVENTORWARE FE solutions. Section VII summarizes conclusions of this paper. In Appendix A, we briefly outline the MoM used in Section III. In Appendix B, we recall the fundamentals of the GMLS approximation.

II. Model Development

We consider a narrow microbeam of length ℓ, width b, and thickness h either clamped–clamped or clamped-free, as depicted in Fig. 1. The microbeam is suspended above an infi-

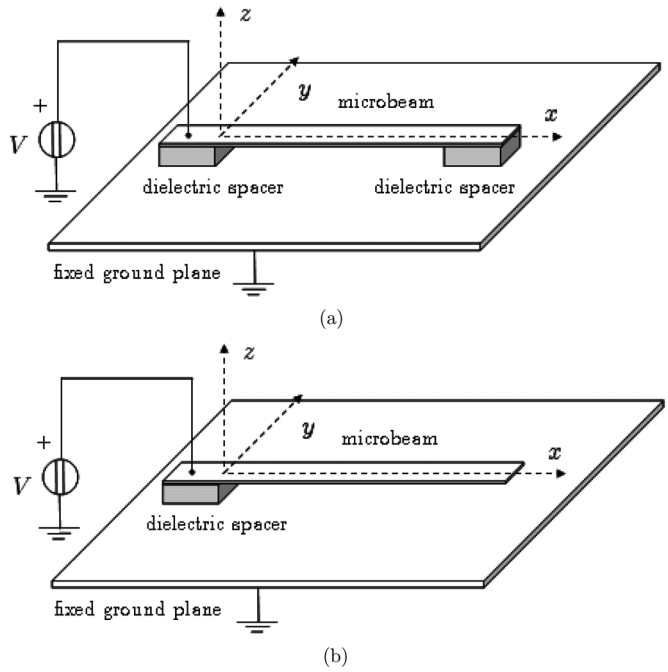

Fig. 1. Electrostatically actuated (a) clamped–clamped and (b) cantilever microbeams.

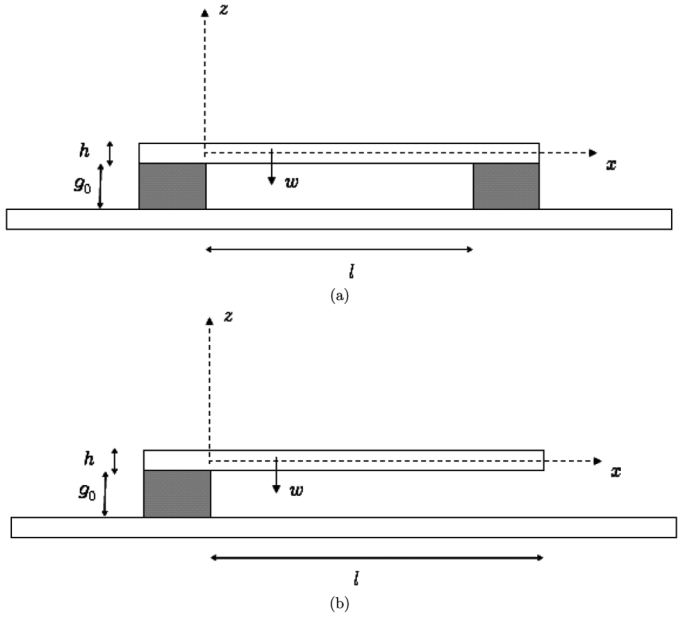

Fig. 2. Side view of the two microbeams: (a) clamped–clamped and (b) cantilever.

nite ground plane with an initial gap g_0. Both bodies are perfect conductors and are separated by a dielectric medium of permittivity $\epsilon_0\epsilon_r$, where ϵ_0 is the vacuum permittivity and ϵ_r is the relative permittivity. A positive potential difference V between the two conductors causes the microbeam to electrostatically deflect downwards.

A. Governing Equation for Mechanical Deformations

Within the large deflection beam theory, see, e.g., [9], the deflection w in the z-direction is given by (see Fig. 2)

$$EI\frac{d^4w}{dx^4} - N(w)\frac{d^2w}{dx^2} = \tilde{F}_e(w) \tag{1}$$

where E is Young's modulus, I is the moment of inertia of the cross section about the y axis, N is the axial force which is constant along the beam axis, $\tilde{F}_e$ is the deflection-dependent electrostatic force per unit length, and x is the axial coordinate. A beam is considered narrow, when its width b is less than five times its thickness h, see, e.g., [8]. For wide beams, the mechanical stiffness EI should be modified as given in [8].

For a cantilever beam, the axial force vanishes, while for a clamped–clamped beam it is given by

$$N(w) = \frac{EA}{2\ell}\int_0^\ell \left(\frac{dw}{dx}\right)^2 dx + N_0$$

where A is the area of the cross section of the beam, and N_0 is the residual axial load. For a narrow beam, the residual axial load is $N_0 = \tilde{\sigma}A$, where $\tilde{\sigma}$ is the effective residual axial stress. The residual stress is equal to $\sigma_0(1-\nu)$, where σ_0 is the initial uniform biaxial stress in the material, see, e.g., [8], and ν is Poisson's ratio for the material of the beam.

For a fixed-fixed beam, the deflection is subjected to the following four kinematic boundary conditions:

$$\begin{aligned} w(0) &= 0 \\ \frac{dw}{dx}(0) &= 0 \\ w(\ell) &= 0 \\ \frac{dw}{dx}(\ell) &= 0 \end{aligned} \tag{2}$$

while for a cantilever beam the deflection should satisfy the two kinematic boundary conditions at the clamped end, and the two kinetic boundary conditions at the free end $x = \ell$

$$\begin{aligned} w(0) &= 0 \\ \frac{dw}{dx}(0) &= 0 \\ \frac{d^2w}{dx^2}(\ell) &= 0 \\ \frac{d^3w}{dx^3}(\ell) &= 0. \end{aligned} \tag{3}$$

B. Distributed Force Due to Electric Field

The distributed force $\tilde{F}_e(w)$ on the deformable microbeam due to the electric field depends on the potential difference between the two conductors and on their geometries. Since only small deformations of the beam are considered, it is reasonable to assume that at every point x the electrostatic force per unit length $\tilde{F}_e$ depends only on the local deflection $w(x)$ and equals the force per unit length acting on an infinitely long straight beam separated by a distance $g(x) = g_0 - w(x)$ from a ground

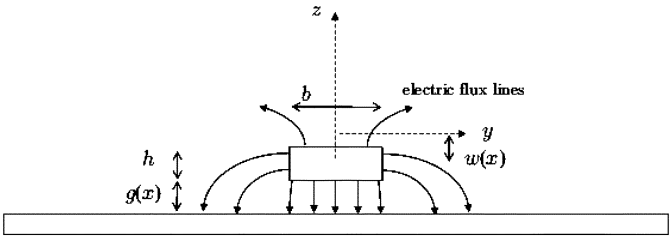

Fig. 3. Schematic view of the beam cross section with grounded electrode.

plane, as shown in Fig. 3. The $\tilde{F}_e$ may be computed by differentiating the energy per unit length stored in the capacitor with respect to the gap g, i.e.,

$$\tilde{F}_e = -\frac{1}{2}V^2\frac{\partial C_g}{\partial g}.$$

Here, C_g is the capacitance per unit length of the 2-D conductors' system and V is the voltage difference between the two plates. The capacitance C_g is comprised of the parallel-plate capacitance, the fringing field capacitance due to the finite width, and the finite thickness of the beam.

C. Dimensionless Governing Equations

For convenience we introduce the nondimensional deflection $\hat{w} = w/g_0$ and the nondimensional abscissa $\hat{x} = x/\ell$. In terms of nondimensional variables, (1) becomes

$$\frac{d^4\hat{w}}{d\hat{x}^4}(\hat{x}) - \left[N_1\int_0^1\left(\frac{d\hat{w}}{d\hat{x}}\right)^2 d\hat{x} + \hat{N}_0\right]\frac{d^2\hat{w}}{d\hat{x}^2}(\hat{x}) = \hat{F}_e(\hat{w}(\hat{x}))$$

where for a clamped–clamped beam

$$N_1 = 6\frac{g_0^2}{h^2}$$
$$\hat{N}_0 = \frac{N_0\ell^2}{EI} = 12\frac{\tilde{\sigma}\ell^2}{Eh^2},$$
$$\hat{F}_e(\hat{w}(\hat{x})) = \frac{12\ell^4}{Eg_0bh^3}\tilde{F}_e(w(x))$$

and for a cantilever beam

$$N_1 = \hat{N}_0 = 0.$$

The capacitance per unit length C_g may be expressed as

$$C_g = C_g^0\mathcal{F}(\beta,\eta) \tag{4}$$

where $\mathcal{F}$ represents the fringing field function, and

$$C_g^0 = \epsilon_0\epsilon_r\frac{b}{g} \tag{5}$$

is the capacitance per unit length when all fringing effects are neglected, and

$$\beta = \frac{h}{b}, \quad \eta = \frac{h}{g}. \tag{6}$$

Therefore, the dimensionless electrostatic force is

$$\hat{F}_e = \frac{\mu}{(1-\hat{w})^2}\left(\mathcal{F} + \eta\frac{\partial\mathcal{F}}{\partial\eta}\right)$$

where the electrostatic load parameter μ is given by

$$\mu = \frac{6\ell^4\epsilon_0\epsilon_r V^2}{Eh^3g_0^3}.$$

In Section III, we will derive an expression for $\hat{F}_e$ applicable to a narrow microbeam.

Henceforth, we drop the superimposed hat on dimensionless variables and use a prime to indicate derivative with respect to the dimensionless axial coordinate. Therefore, the governing equation (1) in terms of nondimensional variables is

$$w^{IV}(x) - N(w)w''(x) = F_e(w(x)) \tag{7}$$

where for a clamped–clamped beam

$$N(w) = N_1\int_0^1 (w')^2 dx + N_0$$

and for a cantilever beam

$$N(w) = 0.$$

D. Weak Formulation

For a clamped–clamped microbeam, we introduce the following weak formulation (see, e.g., [26]) of the problem described by the governing equation (7) and the nondimensional version of the boundary conditions (2):

$$\begin{aligned}0 = &\int_0^1 w''\tilde{w}''dx + N(w)\int_0^1 w'\tilde{w}'dx - \int_0^1 F_e\tilde{w}dx\\ &+ (\lambda_1\tilde{w}(0) + \lambda_2\tilde{w}'(0) + \lambda_3\tilde{w}(1) + \lambda_4\tilde{w}'(1))\\ &+ (\tilde{\lambda}_1 w(0) + \tilde{\lambda}_2 w'(0) + \tilde{\lambda}_3 w(1) + \tilde{\lambda}_4 w'(1)).\end{aligned} \tag{8}$$

Here, λ_1, λ_2, λ_3, and λ_4 are Lagrange multipliers used to impose the four kinematic boundary conditions (2), $\tilde{w}$ is a smooth test function which does not need to satisfy the kinematic boundary conditions, and $\tilde{\lambda}_1$, $\tilde{\lambda}_2$, $\tilde{\lambda}_3$, and $\tilde{\lambda}_4$ are arbitrary scalar numbers.

For a cantilever microbeam, (8) becomes

$$\begin{aligned}\int_0^1 w''\tilde{w}''dx - \int_0^1 F_e\tilde{w}dx + (\lambda_1\tilde{w}(0) + \lambda_2\tilde{w}'(0))\\ +(\tilde{\lambda}_1 w(0) + \tilde{\lambda}_2 w'(0)) = 0\end{aligned} \tag{9}$$

where only two Lagrange multipliers are employed since only two kinematic boundary conditions are prescribed.

The consideration of Lagrange multipliers allows for the simultaneous application of the MLPG and the FE methods. Indeed, the GMLS basis functions (see Appendix B) used in the MLPG method do not have the Kronecker delta property, see, e.g., [13], and special techniques, such as Lagrange multipliers, are needed to enforce kinematic boundary conditions.

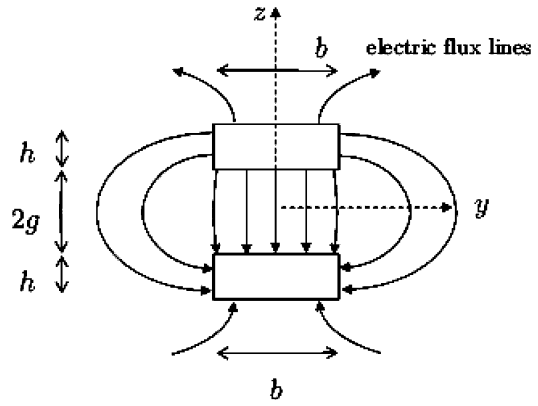

Fig. 4. System of auxiliary conductors for computing the electrostatic capacitance.

III. Computation of the Electric Force Field

The problem of computing the capacitance per unit length of the present system of conductors has been addressed in the literature on semiconductor-integrated circuits [27] and microwave striplines [28]. Several empirical and analytical expressions have been proposed, but none of them seem to be applicable to a narrow microbeam.

We derive here an empirical formula for the capacitance per unit length of the line to ground system, shown in Fig. 3, for a narrow microbeam. The empirical formula is based on a least-square fitting of numerical values obtained by using the well-known MoM, see, e.g., [24], outlined in Appendix A for piecewise constant basis functions and the collocation method.

A. Empirical Formula for the Capacitance

The capacitance C_g of the line to ground system of Fig. 3 equals twice the capacitance $\bar{C}_g$ of two identical rectangular conductors depicted in Fig. 4. Therefore, we consider this auxiliary system involving finite size conductors and exploit symmetry conditions.

By using the MoM, we numerically computed the capacitance per unit length C_g for different values of dimensionless parameters β and η defined in (6) ranging from 0.2 to 2 and 0.4 to 5, respectively. The resulting data are then least-squares fitted by a function of the following form:

$$C_g = \epsilon_0 \epsilon_r \left(\frac{\eta}{\beta} + c_0 + c_1 \left(\frac{\eta}{\beta} \right)^{c_2} + c_3 \eta^{c_4} \right) \tag{10}$$

where c_0, c_1, c_2, c_3, and c_4 are constants. The first term on the right-hand side of (10) describes the parallel-plate capacitance, the third term accounts for the fringing field capacitance due to the finite width b, and the fourth term models the fringing field capacitance due to the finite thickness. Numerical values of the optimized constants are

$$\begin{aligned} c_0 &= -0.36 \\ c_1 &= 0.85 \\ c_2 &= 0.24 \\ c_3 &= 2.5 \\ c_4 &= 0.24. \end{aligned} \tag{11}$$

In the chosen range of variation for β and η, the maximum deviation in the capacitance between the empirical estimate obtained by substituting from (11) into (10) and the fully converged numerical solution achieved by using the MoM is less than 2%. Therefore, the fringing field function that we propose to use in (4) is

$$\mathcal{F}(\beta, \eta) = 1 - 0.36 \frac{\beta}{\eta} + 0.85 \left(\frac{\beta}{\eta} \right)^{0.76} + 2.5 \frac{\beta}{\eta^{0.76}}. \tag{12}$$

B. Validation of the Capacitance Estimate

In Table I, we compare capacitance values computed from (4) by substituting the expression for the fringing field $\mathcal{F}(\beta, \eta)$ from relation (12) and from relations available in the literature, i.e., Palmer's formula [29],

$$\mathcal{F}(\beta, \eta) = 1 + \frac{2}{\pi} \frac{\beta}{\eta} \left(1 + \ln \left(\pi \frac{\eta}{\beta} \right) \right) \tag{13}$$

the parallel-plate approximation $\mathcal{F}(\beta, \eta) = 1$, and the Meijs-Fokkema relation [30]

$$\mathcal{F}(\beta, \eta) = 1 + 0.77 \frac{\beta}{\eta} + 1.06 \left(\frac{\beta}{\eta} \right)^{0.75} + 1.06 \frac{\beta}{\eta^{0.5}}. \tag{14}$$

We use a fully converged solution obtained with the MoM for comparing accuracies of different formulas. It is clear that, for narrow microbeams with $0.5 \leq b/h \leq 5$, $0.2 \leq g/h \leq 2$, the Palmer formula and the parallel-plate approximation give erroneous values of the capacitance per unit line. As stated in [30], values from the Meijs–Fokkema formula have a maximum deviation of 2% for $\eta/\beta = b/g \geq 1$, $0.1 \leq \eta = h/g \leq 4$, and of 6% for $\eta/\beta \geq 0.3$ and $\eta < 10$. The estimate is worst when the gap size is larger than the beam width, i.e., $g/b > 1$. In this case, the error in the capacitance values from the Meijs–Fokkema formula is $\sim 6\%$, which is usually unacceptable. It is also evident that the proposed empirical formula provides accurate estimates for values of β and η that are outside the range of their values used for least-squares fitting.

In Fig. 5(a) and (b), we have plotted the percentage error in the capacitance versus the gap/thickness for $\beta = h/b = 0.2$ (narrow beam) and $\beta = 2$ (significantly narrow beam) computed with the different formulas, and taking as reference the converged numerical values obtained by applying the MoM. As expected, the present interpolation formula (12) provides accurate results for both values of β. The Mejis–Fokkema relation (14) gives precise results for a narrow beam but has moderate discrepancies for a significantly narrow beam. The Palmer expression (13) and the parallel-plate approximation, which totally neglect finite thickness of the beam, provide poor estimates of the electric capacitance for narrow and significantly narrow microbeams. The electrostatic force estimated from the two methods is acceptable only for small gaps. Since the gap varies as the beam deforms, formulas (13) and (14) may not give accurate values of the pull-in voltage.

IV. 1-DOF Model

A closed-form solution of the boundary-value problem defined by (7) and the pertinent boundary conditions cannot be found. Here we give an approximate solution based on a 1-DOF model of the MEMS. The approximate solution is constructed by expressing the dimensionless deflection field as the product

TABLE I
COMPARISON BETWEEN THE CAPACITANCES PER UNIT LENGTH COMPUTED BY THE MOM WITH THOSE FROM (4) BY SUBSTITUTING INTO IT (12) FOR THE FRINGING FIELD AND FROM THREE FORMULAS AVAILABLE IN THE LITERATURE

Geometry		MoM	% Deviations			
β	η	$C_g/(\epsilon_0\epsilon_r)$	Eq. (12)	Meijs-Fokkema (eq. (14))	Palmer (eq. (13))	Parallel-Plate
0.1	0.5	8.14	−1.6	−0.4	−9.2	−38.6
0.1	1	13.71	−0.7	< 0.1	−6.5	−27.1
0.1	2.5	29.61	< 0.1	0.7	−4.1	−15.7
0.1	5	55.38	0.2	1.0	−3.0	−9.9
0.1	10	106.19	0.3	1.2	2.2	−6.2
0.2	0.5	5.37	−1.1	−0.4	−17.2	−53.5
0.2	1	8.42	−0.4	−0.1	−12.3	−40.7
0.2	2.5	16.80	< 0.1	0.8	−8.0	−25.6
0.2	5	30.06	0.3	1.5	−5.6	−16.9
0.2	10	55.86	0.5	1.9	−4.0	−10.9
0.5	0.5	3.61	< 0.1	−0.8	−34.5	−72.3
0.5	1	5.12	0.4	−0.6	−25.7	−61.0
0.5	2.5	8.97	0.4	−0.7	−17.7	−44.3
0.5	5	14.71	0.6	2.1	−12.9	−32.1
0.5	10	25.50	0.9	3.4	−9.1	−21.9
1	0.5	2.96	0.6	−1.7	−51.9	−83.1
1	1	3.96	0.7	−1.8	−40.3	−74.8
1	2.5	6.29	0.4	−0.1	−29.3	−60.2
1	5	9.52	0.5	2.2	−22.4	−47.5
1	10	15.30	1.1	4.6	−16.4	−34.9
2	0.5	2.59	0.8	−2.9	−71.8	−90.4
2	1	3.34	0.7	−3.5	−57.3	−85.0
2	2.5	4.90	< 0.1	−1.7	−43.8	−74.5
2	5	6.88	< 0.1	1.4	−53.3	−63.7
2	10	10.16	0.7	5.4	−27.4	−50.9
5	0.5	2.34	0.3	−5.2	∞	−95.7
5	1	2.92	−0.1	−6.2	−81.5	−93.2
5	2.5	4.03	−1.4	−4.8	−64.7	−87.6
5	5	5.25	−1.6	−1.0	−55.0	−81.0
5	10	7.04	−0.7	4.9	−45.9	−71.6

of an unknown deflection parameter ζ and a given trial function $\bar{w}(x)$ satisfying the kinematic boundary conditions

$$w(x) = \zeta \bar{w}(x). \tag{15}$$

The governing equation for ζ is derived by multiplying both sides of (7) by $\bar{w}$, integrating over the beam span, and substituting into the resulting equation the approximate solution (15). After integrating by parts, the governing equation for ζ becomes

$$(k_0 + k_1)\zeta + k_2\zeta^3 = \mu f_e(\zeta) \tag{16}$$

where

$$k_0 = \int_0^1 (\bar{w}''(x))^2 dx$$

$$k_1 = N_0 \int_0^1 (\bar{w}'(x))^2 dx$$

$$k_2 = N_1 \left(\int_0^1 (\bar{w}'(x))^2 dx \right)^2$$

$$f_e(\zeta) = \frac{1}{\mu} \int_0^1 F_e(\zeta \bar{w}(x)) \bar{w}(x) dx.$$

Note that F_e is linear in μ, therefore, f_e is independent of μ. The left-hand side of (16) represents the restoring elastic force, while the right-hand side the electrostatic force. Furthermore, the term multiplying ζ represents the stiffness of a linear elastic beam and that multiplying ζ^3 the strain-stiffening effect. The lumped electrostatic force depends on the adopted fringing field correction, and it cannot in general be expressed analytically. Note that (15) gives the admissible equilibrium states of the system. As the parameter μ increases from zero the overall stiffness of the system decreases and it vanishes at the pull-in instability. Therefore, pull-in occurs in an equilibrium state for which the first derivative of the equilibrium (16) with respect to the deflection parameter ζ vanishes.

This implies that the pull-in deflection and voltage should satisfy simultaneously (16), and its derivative with respect to ζ, i.e.,

$$(k_0 + k_1) + 3k_2\zeta^2 = \mu \frac{df_e(\zeta)}{d\zeta}. \tag{17}$$

By eliminating μ from (16) and (17), we obtain

$$f_e(\zeta)\left((k_0 + k_1) + 3k_2\zeta^2\right) - \frac{df_e(\zeta)}{d\zeta}\left((k_0 + k_1)\zeta + k_2\zeta^3\right) = 0. \tag{18}$$

By solving (18) for ζ, and by substituting the value of ζ into (16), we determine the pull-in instability parameters, i.e., deflection

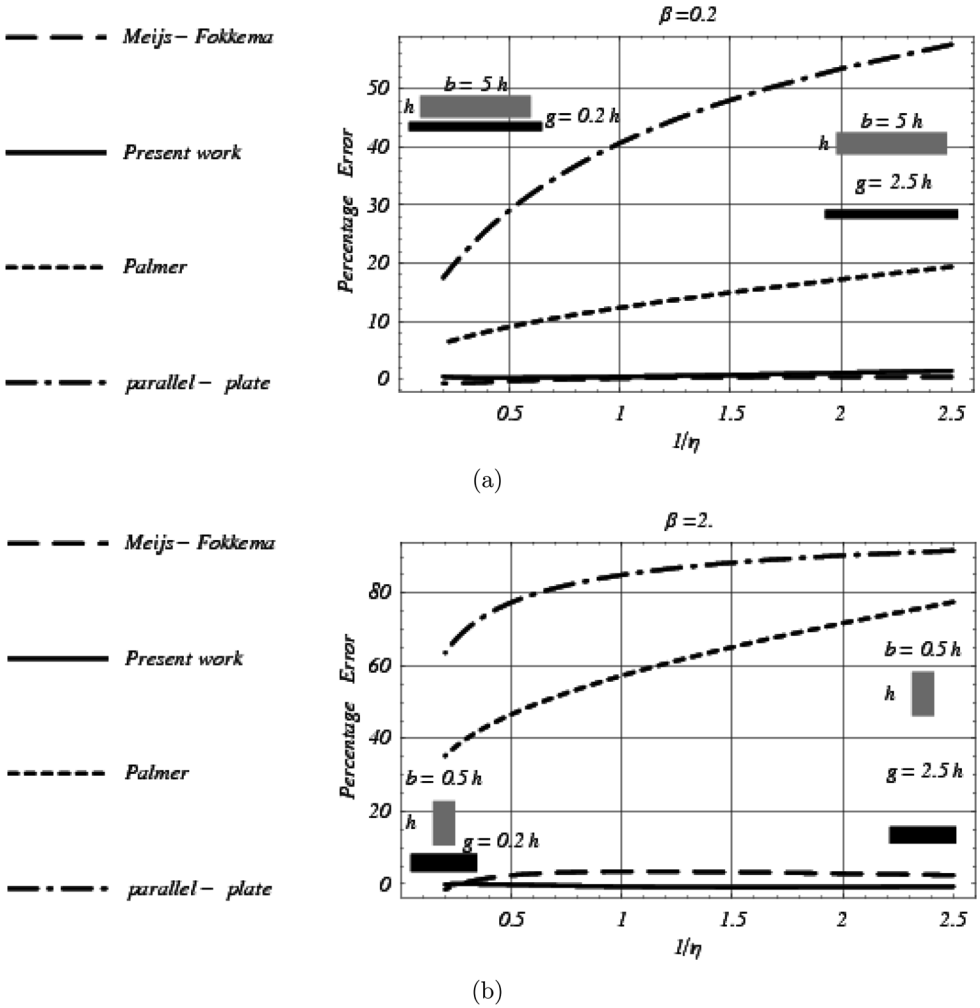

Fig. 5. Taking the capacitance computed with the MoM as reference, comparison of the error in the capacitance per unit length for a narrow microbeam obtained with different methods.

and voltage. We emphasize that, once the trial function $\bar{w}(x)$ has been chosen, (18) reduces to a nonlinear algebraic equation for ζ, where the derivative $df_e(\zeta)/d\zeta$ can be computed for any ζ by numerical integration. In general, (16) cannot be solved analytically, and standard root finding techniques such as the bisection algorithm (see, e.g., [31]) may be applied.

When k_2 is different from zero, fringing fields are taken into account and arbitrary trial functions are used, multiple solutions may be present. We determine the pull-in parameters by considering the lowest root of (18). In our numerical simulations, we found that (18) has one solution.

We choose as a trial function $\bar{w}(x)$ the normalized linear static deflection of the microbeam due to a uniformly distributed applied load. Therefore, for a clamped–clamped microbeam, we take

$$\bar{w}(x) = 16x^2(1-x)^2$$

and consequently

$$\begin{aligned} k_0 &= \frac{1024}{5} \\ k_1 &= N_0 \frac{512}{105} \\ k_2 &= N_1 \left(\frac{512}{105}\right)^2. \end{aligned}$$

For a cantilever microbeam, we choose

$$\bar{w}(x) = \frac{1}{3}x^2(6-4x+x^2)$$

thus

$$\begin{aligned} k_0 &= \frac{16}{5} \\ k_1 &= 0 \\ k_2 &= 0. \end{aligned}$$

In the beam's undeformed configuration, the electrostatic force acts as a uniformly distributed load, and the nonlinear mechanical stiffness is zero. Therefore, the chosen trial function represents the actual microbeam deflection when small voltages are involved. Moreover, from the analysis of the distributed model with the MLPG and the FE methods, it appears that the shape of the deformed beam does not change appreciably as the voltage is increased. These ensure the effectiveness of the present choice, which is validated by numerical results presented in Section VI.

V. Numerical Methods

A. Discrete Nonlinear Formulation

In order to seek an approximate solution of the nonlinear problem, we find the deflection by using either the MLPG

method with the GMLS basis functions [15] outlined in Appendix B or the FE method with the Hermite polynomial basis functions [32]. In both cases, indicating by N the number of nodes on the beam, the trial solution is expressed as

$$w^h(x) = \boldsymbol{\psi}(x)^T \hat{\mathbf{s}} \tag{19}$$

where $\boldsymbol{\psi}(x)$ is a $2N$ vector comprised of the basis functions, and $\hat{\mathbf{s}}$ is the vector of $2N$ nodal unknowns. For the GMLS approximation, $\hat{\mathbf{s}}$ represents the fictitious nodal values [15]. The number of unknowns in the problem is $2N + N_{L,}$ where N_L is the number of Lagrange multipliers. From (8) and (9), N_L equals 4 for a clamped-clamped beam, and 2 for a cantilever beam. By substituting the approximation (19) into either (8) or (9), by considering displacement test functions of the form

$$\tilde{w} = \boldsymbol{\gamma}\boldsymbol{\psi}(x)$$

where $\boldsymbol{\gamma}$ is a $2N$ row vector of arbitrary constants, and by introducing a N_L vector $\tilde{\boldsymbol{\lambda}}$ of arbitrary constants, we get the following discrete nonlinear equations:

$$\mathbf{K}(\hat{\mathbf{s}})\hat{\mathbf{s}} + \mu\mathbf{G}(\hat{\mathbf{s}}) + \mathbf{V}^T\boldsymbol{\lambda} = \mathbf{0} \tag{20a}$$

$$\mathbf{V}\hat{\mathbf{s}} = \mathbf{0} \tag{20b}$$

where

$$\begin{aligned}
\mathbf{K}(\hat{\mathbf{s}}) &= \int_0^1 \boldsymbol{\psi}''(x)\boldsymbol{\psi}''(x)^T dx \\
&\quad + N(\boldsymbol{\psi}(x)^T\hat{\mathbf{s}}) \\
&\quad \times \int_0^1 \boldsymbol{\psi}'(x)\boldsymbol{\psi}'(x)^T dx \\
\mathbf{G}(\hat{\mathbf{s}}) &= -\frac{1}{\mu}\int_0^1 F_e(\boldsymbol{\psi}(x)^T\hat{\mathbf{s}})\boldsymbol{\psi}(x)dx \\
\text{clamped-clamped}: V_{1i} &= \psi_i(0), \quad V_{2i} = \psi_i'(0) \\
V_{3i} &= \psi_i(1), \quad V_{4i} = \psi_i'(1) \\
\boldsymbol{\lambda} &= [\lambda_1\ \lambda_2\ \lambda_3\ \lambda_4]^T \\
\text{cantilever}: V_{1i} &= \psi_i(0), \quad V_{2i} = \psi_i'(0) \\
\boldsymbol{\lambda} &= [\lambda_1\ \lambda_2]^T
\end{aligned}$$

and $i = 1, \ldots, 2N$.

Let rows of the $(2N - N_L) \times 2N$ matrix $\mathbf{Y}$ be comprised of $(2N - N_L)$ linearly independent null vectors of the $N_L \times 2N$ matrix $\mathbf{V}$, and set

$$\hat{\mathbf{s}} = \mathbf{Y}^T\mathbf{s}. \tag{21}$$

Substitution from (21) into (20b) gives

$$\mathbf{V}\mathbf{Y}^T\mathbf{s} = \mathbf{0}$$

which are identically satisfied for every $(2N - N_L)$-vector $\mathbf{s}$. Premultiplying both sides of (20a) by $\mathbf{Y}$ and substituting from (21), we obtain the following reduced system of $(2N - N_L)$ nonlinear equations for $\mathbf{s}$:

$$\bar{\mathbf{K}}(\mathbf{s})\mathbf{s} + \mu\bar{\mathbf{G}}(\mathbf{s}) = \mathbf{0} \tag{22}$$

where

$$\begin{aligned}
\bar{\mathbf{K}}(\mathbf{s}) &= \mathbf{Y}\mathbf{K}(\mathbf{Y}^T\mathbf{s})\mathbf{Y}^T \\
\bar{\mathbf{G}}(\mathbf{s}) &= \mathbf{Y}\mathbf{G}(\mathbf{Y}^T\mathbf{s}).
\end{aligned}$$

Having found $\mathbf{s}$ from (22), $\hat{\mathbf{s}}$ is computed from (21).

B. DIPIE Algorithm

We use the DIPIE algorithm (see, e.g., [23]) to solve the set of equations (22) and find the complete bifurcation path. It treats the applied voltage as an additional unknown, using the deflection $\bar{w}$ of a prechosen beam point $\bar{x}$ as the driving parameter for the iteration scheme. In this way, the original problem, which has both stable and unstable equilibrium states, is replaced by a sequence of equivalent problems.

If the deflection $\bar{w}_{k-1}$ is known, the solution $(\mathbf{s}_k, \mu_k) = (\mathbf{s}_{k-1} + \Delta\mathbf{s}_k, \mu_{k-1} + \Delta\mu_k)$ at the deflection $\bar{w}_k = \bar{w}_{k-1} + \Delta\bar{w}_k$ is found by solving the system of equations

$$\bar{\mathbf{K}}(\mathbf{s}_k)\mathbf{s}_k + \mu_k\bar{\mathbf{G}}(\mathbf{s}_k) = \mathbf{0} \tag{23a}$$

$$\boldsymbol{\psi}(\bar{x})^T\mathbf{Y}^T\mathbf{s}_k = \boldsymbol{\psi}(\bar{x})^T\mathbf{Y}^T\mathbf{s}_{k-1} + \Delta\bar{w}_k. \tag{23b}$$

The solution of the set of nonlinear equations (23), in terms of the unknowns Δs_k and $\Delta\mu_k$, is found by using Newton's iterations. Hence, at the generic τth iteration

$$\begin{bmatrix} \bar{\mathbf{T}}_k^{(\tau)}\left(\mathbf{s}_k^{(\tau)}\right) & \bar{\mathbf{G}}\left(\mathbf{s}_k^{(\tau)}\right) \\ \boldsymbol{\psi}(\bar{x})^T\mathbf{Y}^T & 0 \end{bmatrix} \begin{bmatrix} \Delta\mathbf{s}_k^{(\tau)} \\ \Delta\mu_k^{(\tau)} \end{bmatrix} = -\begin{bmatrix} \bar{\mathbf{K}}\left(\mathbf{s}_k^{(\tau)}\right)\mathbf{s}_k^{(\tau)} + \mu_k^{(\tau)}\bar{\mathbf{G}}\left(\mathbf{s}_k^{(\tau)}\right) \\ \boldsymbol{\psi}(\bar{x})^T\mathbf{Y}^T\mathbf{s}_k^{(\tau)} - \Delta\bar{w}_k \end{bmatrix}$$

where $\left(\Delta\mathbf{s}_k^{(\tau)}, \Delta\mu_k^{(\tau)}\right)$ indicates the τth solution increment; $\left(\mathbf{s}_k^{(\tau)}, \mu_k^{(\tau)}\right)$ is the updated solution at the $(\tau - 1)$th iteration, i.e.

$$\mathbf{s}_k^{(\tau)} = \mathbf{s}_{k-1} + \sum_{h=1}^{\tau-1}\Delta\mathbf{s}_k^{(h)}, \quad \mu_k^{(\tau)} = \mu_{k-1} + \sum_{h=1}^{\tau-1}\Delta\mu_k^{(h)}$$

and $\mathbf{T}_k^{(\tau)}\left(\mathbf{s}_k^{(\tau)}\right)$ is the tangent stiffness at the $(\tau-1)$th iteration, i.e.

$$\begin{aligned}
\mathbf{T}_k^{(\tau)}\left(\mathbf{s}_k^{(\tau)}\right) &= \int_0^1 \boldsymbol{\psi}''(x)\boldsymbol{\psi}''(x)^T dx \\
&\quad + 2N_1\int_0^1 \left(\boldsymbol{\psi}'(x)^T\mathbf{Y}^T\mathbf{s}_k^{(\tau)}\right)\boldsymbol{\psi}'(x)dx \\
&\quad \times \int_0^1 \boldsymbol{\psi}'(x)^T\left(\boldsymbol{\psi}'(x)^T\mathbf{Y}^T\mathbf{s}_k^{(\tau)}\right)dx \\
&\quad + \mu^{(\tau)}\mathbf{Y}\mathbf{D}_k^{(\tau)}\mathbf{Y}^T
\end{aligned}$$

with

$$\mathbf{D}_k^{(\tau)} = -\int_0^1 \frac{\partial F_e}{\partial w^h}\left(\boldsymbol{\psi}(x)^T\mathbf{Y}^T\mathbf{s}_k^{(\tau)}\right)\boldsymbol{\psi}(x)\boldsymbol{\psi}(x)^T dx.$$

The iterations are performed until the infinity norm of the incremental solution, i.e., its maximum value over the beam span satisfies

$$\max_{x\in(0,1)}\left[\boldsymbol{\psi}(x)^T\mathbf{Y}^T\Delta\mathbf{s}_k^{(\tau)}\right]\leq\varepsilon_k$$

where

$$\varepsilon_k=\varepsilon^A+\varepsilon^R\max_{x\in(0,1)}\left[\boldsymbol{\psi}(x)^T\mathbf{Y}^T\Delta\mathbf{s}_k^{(1)}\right] \tag{24}$$

and ε^A and ε^R are preassigned small numbers. For a clamped–clamped microbeam, we choose $\bar{x}$ equal to the mid-span, and for a cantilever microbeam, we take $\bar{x}$ equal to the beam length. In order to extract the pull-in parameters, we monitor the electrostatic parameter $\Delta\mu_k$, since pull-in occurs when this parameter changes sign. We use a constant step for iterating the deflection and, if necessary, additional iterations are performed for pull-in parameters.

VI. Results and Comparisons

In [8], the mid-plane stretching and the fringing field capacitance due to the finite thickness of the beam are neglected, and the Palmer approximate formula (13) is used. Therefore, expressions of the dimensionless axial load, and for the dimensionless force per unit length are

$$N=\begin{cases}N_0, & \text{clamped-clamped}\\ 0, & \text{cantilever}\end{cases}$$
$$F_e=\frac{\mu}{(1-w)^2}\left(1+\frac{2}{\pi}\frac{\beta}{\eta}\right). \tag{25}$$

In [9], the mid-plane stretching is considered but all fringing field effects are neglected. Consequently, the electric force per unit length is given by

$$F_e=\frac{\mu}{(1-w)^2}. \tag{26}$$

In [10], the mid-plane stretching is accounted for, and the fringing field effects are treated as in [8].

Here we compare predictions of the models developed in [8]–[10] with those of the present model for two sample problems: a cantilever and a clampled-clamped microbeam. Both geometries have been analyzed in [11] by using the software COVENTORWARE. Recent findings [33] do not agree with the results of [11] for the clamped–clamped beam. Moreover, for the problem analyzed in [11], the microbeam deflections are relatively small, the nonlinear stiffening does not seem significant, and the numerical findings do not include the pull-in deflection which is a crucial design parameter.

Therefore, we performed our own 3-D FE simulation using ANSYS. Details of the performance of simulating MEMS problems with ANSYS are given in [34]. Following guidelines [34] on the accuracy of different simulation options, we used the tool ROM 144. We adapted the "Sample Miniature Clamped–Clamped Beam Analysis" [35, Example 6.6] to a narrow microbeam by extending the surrounding dielectric medium in order to accurately model the fringing fields. The region analyzed and its discretization into FEs are reported in Fig. 6 for the clamped–clamped microbeam; only half of the system is modeled due to symmetry conditions, and a refined mesh is employed in the gap region. In particular, the dielectric medium is considered as a block of length 100 μm, semi-width of 24 μm, and thickness of 24 μm. For the cantilever microbeam problem, the dielectric domain has been also increased along the beam axis by 24 μm in order to model fringing fields at the free end. The elements SOLID 145 (eight-node brick elements) were used to model the microbeam, while SOLID 122 (20-node tetrahedral elements) were used to model the dielectric. Geometric nonlinearities have been included in the simulation. Table II lists the geometry and the material properties of the problems studied. The adopted mesh densities and dielectric region dimensions correspond to the minimum required to obtain a fully converged solution for the pull-in parameters. Indeed, performing numerical experiments by varying both the dielectric region and the mesh density for the beam and the dielectric, we established that the third significant digit of the pull-in voltage and the pull-in deflection does not change either considering a more refined mesh or a larger dielectric domain.

While using (22), a uniform grid of nine uniformly spaced nodes has been used for both the MLPG and the FE methods, and results were found to be practically indistinguishable from those obtained by considering more nodes. Numerical integrations have been performed by using 10 Gauss quadrature

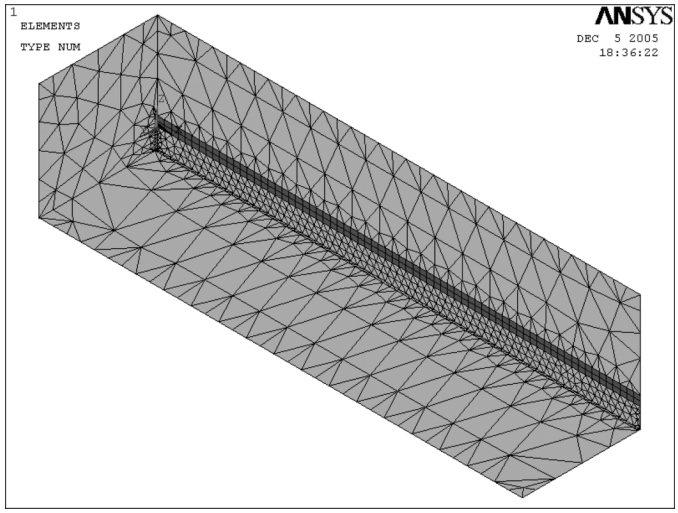

Fig. 6. Schematics of the 3-D FE mesh used for ANSYS simulations of the clamped–clamped beam. The domain in light gray is the dielectric, and the one in dark gray is the microbeam.

TABLE II
Geometric and Material Parameters for the Problems Studied. For the Cantilever Beam Problem, Case (1) Refers to the Geometry Analyzed Herein With ANSYS, While Case (2) to the Problem Analyzed in [11]

	Clamped-Clamped	Cantilever: case (1)	Cantilever: case (2)
ℓ, [μm]	100	100	300
b, [μm]	1	1	0.5
h, [μm]	2	2	1
g_0, [μm]	4	4	2.5
E, [GPa]	169	169	77
ν	0.066	0.066	0.33
ϵ_r	1	1	1

TABLE III
COMPARISON OF PULL-IN VOLTAGES, V_{PI}, AND PULL-IN DEFLECTIONS INFINITY NORM, $\|w_{PI}\|_\infty$, OF THE CLAMPED-CLAMPED MICROBEAM OBTAINED FROM DIFFERENT MODELS, DIFFERENT METHODS, AND WITH THE INITIAL STRESS, σ_0, EQUAL TO (A) $\sigma_0 = 100$ MPa, (B) $\sigma_0 = 0$, AND (C) $\sigma_0 = -100$ MPa. THE MLPG AND THE FE REFER TO SOLUTIONS OF THE ONE-DIMENSIONAL BOUNDARY-VALUE PROBLEM WITH THE MLPG AND THE FE METHODS, RESPECTIVELY

(a) $\sigma_0 = 100\,\text{MPa}$

	V_{PI}, [V]			$\|w_{\text{PI}}\|_\infty$, [μm]		
ANSYS	902			2.47		
	1 d.o.f.	MLPG	FE	1 d.o.f	MLPG	FE
Ref. [9]	1513	1510	1510	2.13	2.11	2.11
Ref. [10]	1003	999	1000	2.55	2.53	2.53
Ref. [8]	783	783	783	1.96	1.96	1.96
Present Work	945	942	942	2.48	2.46	2.47

(b) $\sigma_0 = 0\,\text{MPa}$

	V_{PI}, [V]			$\|w_{\text{PI}}\|_\infty$, [μm]		
ANSYS	830			2.57		
	1 d.o.f.	MLPG	FE	1 d.o.f	MLPG	FE
Ref. [9]	1373	1371	1371	2.24	2.23	2.24
Ref. [10]	923	920	920	2.63	2.62	2.62
Ref. [8]	663	660	660	1.96	1.96	1.96
Present Work	868	865	866	2.57	2.56	2.56

(c) $\sigma_0 = -100\,\text{MPa}$

	V_{PI}, [V]			$\|w_{\text{PI}}\|_\infty$, [μm]		
ANSYS	750			2.64		
	1 d.o.f.	MLPG	FE	1 d.o.f	MLPG	FE
Ref. [9]	1225	1223	1224	2.39	2.39	2.39
Ref. [10]	838	836	836	2.73	2.73	2.73
Ref. [8]	516	506	506	1.96	1.97	1.97
Present Work	786	785	785	2.68	2.68	2.68

points located in each element for the FE method and, in each subinterval, partitioning the entire domain [15] for the MLPG method. The GMLS basis functions are generated by complete monomials of degree 3 ($m = 4$); cf. (29) in Appendix B. The radius R of the weight functions in (36) for the GMLS approximation is five times the distance between two adjacent nodes. The power α in (36) is set equal to 5; see [15] for a discussion of the effect of α on the trial function's degree of smoothness. The tuning of parameters for the MLPG analysis stems from the results in [17], where the effect of different parameters are analyzed, and general guidelines are given. As a rule of thumb, increasing any of the parameters α, R, and m results in a more accurate solution but with more computational time. In the DIPIE algorithm for the clamped–clamped microbeam, the increment of the driving parameter $\Delta\bar{w}_k$ equals 2.5×10^{-3}, while for the cantilever microbeam the increments of the driving parameter are 4.0×10^{-3} for case (1) and 1.0×10^{-2} for case (2) in Table II. These choices are motivated by the need to estimate the third significant digit in the dimensional pull-in maximum deflection. The tolerances in Newton's iterations for the DIPIE algorithm are $\varepsilon^A = 10^{-6}$ and $\varepsilon^R = 10^{-4}$; see (24).

Results of different computations on the clamped–clamped microbeam are given in Table III; results of the ANSYS FE simulations are considered to be most reliable since they do

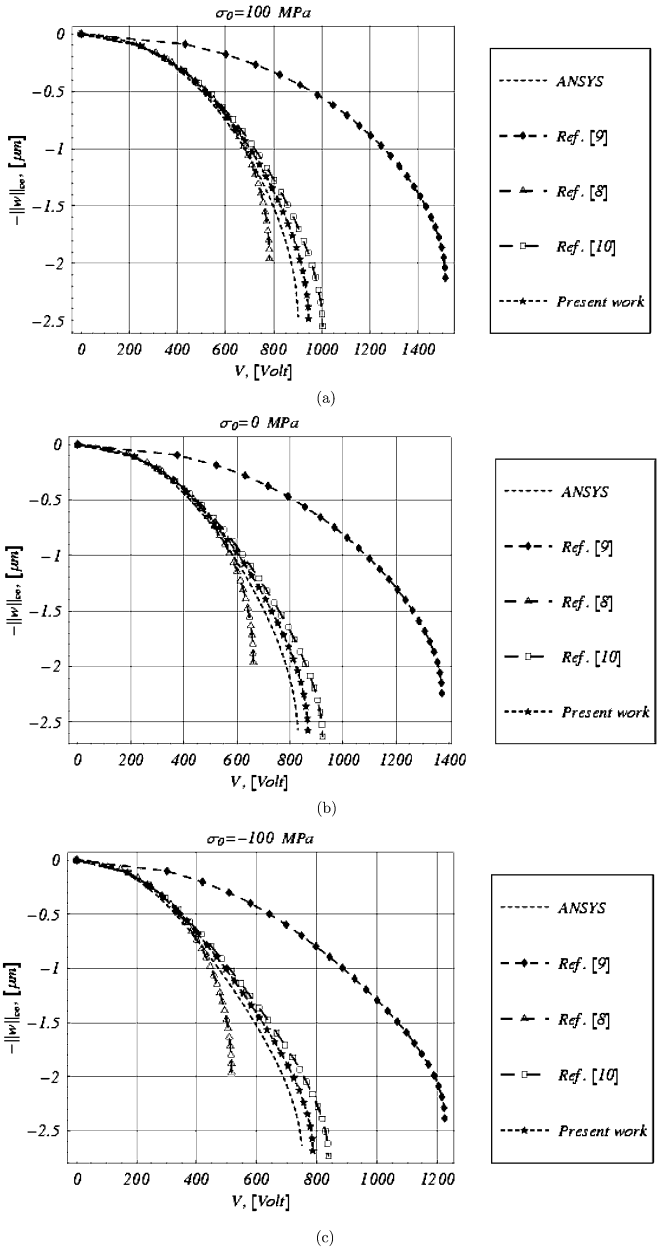

Fig. 7. Plots of the maximum displacement versus the applied voltage for the clamped–clamped microbeam problem under different initial states of stress. Results from all models are reported up to their predicted pull-in instability. (a) $\sigma_0 = 100$ MPa. (b) $\sigma_0 = 0$ MPa. (c) $\sigma_0 = -100$ MPa.

not involve *a priori* assumptions on the mechanical and the electrical behavior of the system. Three different values of the initial stress σ_0, representative of pretensioned, stress-free, and precompressed beams, have been examined. Results for the precompressed beam have been computed by tacitly assuming that the beam is constrained from buckling. Results from models of [8]–[10] have also been computed with the MLPG and the FE methods, and with the corresponding reduced 1-DOF models. The accuracy of the proposed 1-DOF model explained in Section IV can be ascertained by comparing predictions from it with those from the MLPG and the FE methods. The complete neglect of the fringing field effects leads to significant underestimation of the electrostatic force, consequent overestimation of

TABLE IV
COMPARISON OF PULL-IN VOLTAGES AND PULL-IN DEFLECTIONS OF THE CANTILEVER MICROBEAM OBTAINED FROM DIFFERENT MODELS, DIFFERENT METHODS. THE MLPG AND THE FE REFER TO SOLUTIONS OF THE ONE-DIMENSIONAL BOUNDARY-VALUE PROBLEM WITH THE MLPG AND THE FE METHODS, RESPECTIVELY

(a) Beam (1) of Table 2

	$V_{\rm PI}$, [V]			$\|w_{\rm PI}\|_\infty$, [μm]		
ANSYS	93			1.84		
	1 d.o.f.	MLPG	FE	1 d.o.f	MLPG	FE
Ref. [9]	166	165	165	1.79	1.79	1.79
Ref. [8], [10]	102	102	102	2.20	2.19	2.20
Present Work	98	98	98	2.11	2.11	2.11

(b) Beam (2) of Table 2

	$V_{\rm PI}$, [V]			$\|w_{\rm PI}\|_\infty$, [μm]		
COVENTORWARE	1.2			(not available)		
	1 d.o.f.	MLPG	FE	1 d.o.f	MLPG	FE
Ref. [9]	2.18	2.17	2.17	1.12	1.12	1.12
Ref. [8], [10]	1.25	1.25	1.25	1.40	1.40	1.40
Present Work	1.21	1.21	1.21	1.33	1.33	1.33

the pull-in voltage and underestimation of the pull-in deflection as is evident from the results computed with the model in [9]. By introducing into the model of [9] the fringing field (13), as is done in [10], the pull-in voltage and the pull-in deflection are significantly improved; nevertheless, the pull-in voltage is still overestimated due to the neglect of the finite thickness of the beam in the computation of the electrostatic force. Instead, the pull-in deflection computed by using the model of [10] is in good agreement with the ANSYS FE solution. The removal of the mid-plane stretching effect [8] for the clamped–clamped beam significantly decreases the accuracy of the pull-in deflection, since it completely ignores the nonlinear stiffening which for the present geometry $(g_0/h = 2)$ is extremely relevant. The model developed in [8] is based on assuming small deflections of the microbeam, and therefore it is incapable of accurately estimating pull-in parameters for the present geometry. The pull-in voltage is instead underestimated, since, by neglecting the membrane stretching, the overall mechanical compliance is overestimated. As is evident from the results listed in Table III, the present work, by properly accounting for the fringing field effects due to the beam finite thickness, provides a consistent electromechanical theory that gives accurate results for narrow clamped–clamped microbeams undergoing severe displacements. Fig. 7(a)–(c) reports the voltage versus the maximum deflection for the three values of the initial stress obtained using the five models. The curves are computed by using the simple 1-DOF model explained in Section IV. For increasing voltages, the maximum deflections predicted by these models significantly differ; the response predicted by the present model is closest to that given by ANSYS.

Results of computations on the two sample cantilever microbeams whose parameters are listed in Table II are given in Table IV(a) and (b). The discrepancy between the pull-in voltage predicted by [9] and the ones resulting from either ANSYS or COVENTORWARE [11] signifies the importance of fringing fields for a reliable understanding of the pull-in instability in a narrow microbeam. Wherease we computed results with ANSYS, those with COVENTORWARE are

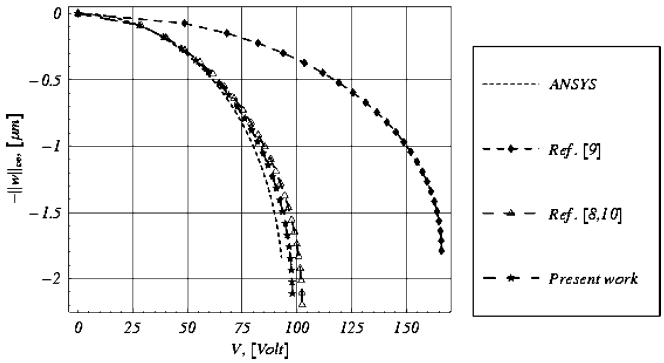

Fig. 8. Plot of the maximum displacement versus the applied voltage for the cantilever microbeam of case (1) in Table II. Results from all models are reported up to their predicted pull-in instability.

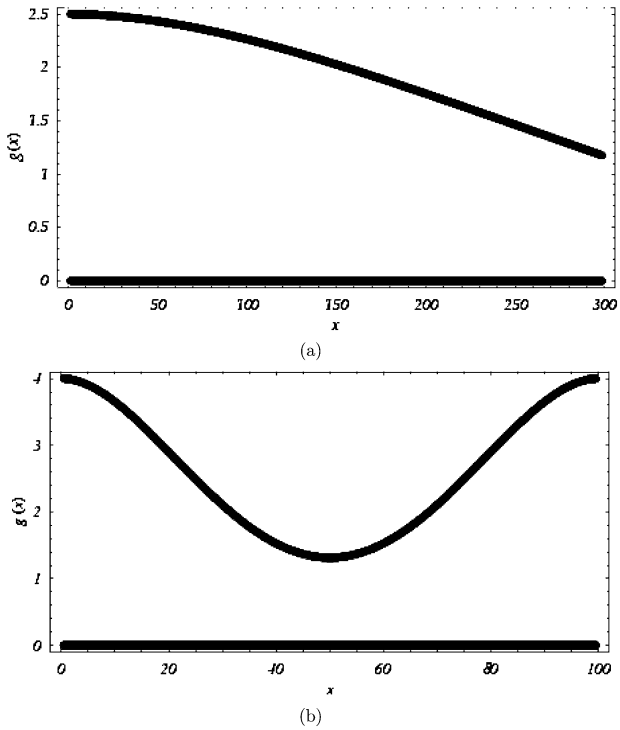

Fig. 9. Deformed shapes of microbeams just prior to the pull-in voltage. Dimensions along the x- and the y-axes are in μm. (a) Cantilever microbeam of case (2), Table II. (b) Clamped-clamped microbeam with $\sigma_0 = 0$ MPa.

from [11]. When compared with the models of [8] and [10], the present model improves both the estimates of the pull-in voltage and the pull-in deflection. Indeed, the models of [8] and [10] underestimate the electrostatic force by neglecting the fringing field effects due to the beam finite thickness and therefore overestimate the pull-in voltage and lead to less accurate estimates of the pull-in deflection. For the five different models, Fig. 8 exhibits the voltage versus the maximum deflection for the geometry identified as case (1) in Table II. The curves are computed by using the simple 1-DOF model presented in Section IV. As for the clamped–clamped microbeam, the complete neglect of fringing fields yields severely erroneous predictions. Accounting for fringing fields in narrow cantilever microbeams dramatically increases the accuracy, and a detailed model of fringing field effects, as has been done in the present work, gives results with relatively low errors.

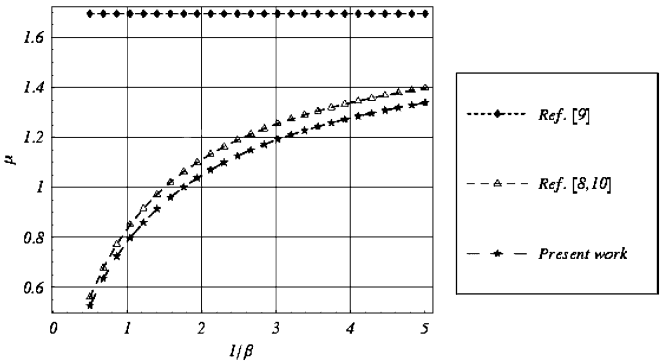

Fig. 10. For the cantilever beam identified as case (2) in Table II, comparison of the nondimensional pull-in voltage μ versus $1/\beta$ computed from the present 1-DOF model with those from [8]–[10].

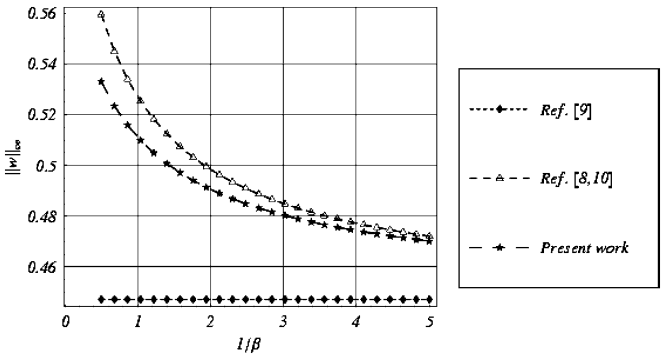

Fig. 12. For the cantilever beam identified as case (2) in Table II, comparison of the maximum pull-in non-dimensional deflection $\|w\|_\infty$ versus $1/\beta$ computed from the present 1-DOF model with those from [8]–[10].

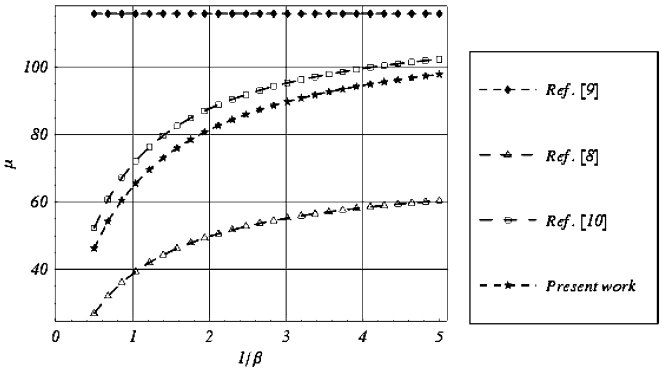

Fig. 11. For the clamped–clamped microbeam of Table II with $\sigma_0 = 0$ MPa, comparison of the non-dimensional pull-in voltage μ versus $1/\beta$ computed from the present 1-DOF model with those from [8]–[10].

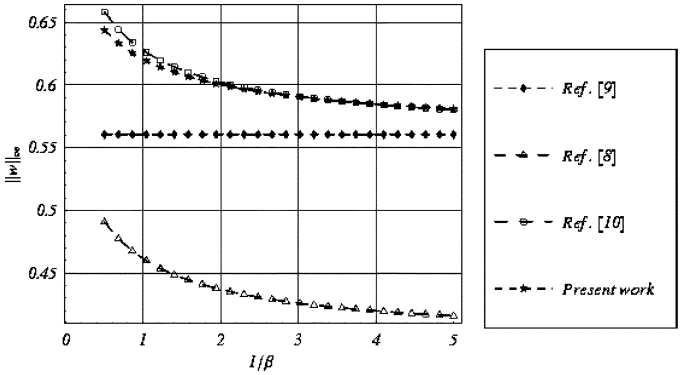

Fig. 13. For the clamped–clamped microbeam described in Table II with $\sigma_0 = 0$ MPa, comparison of the maximum pull-in nondimensional deflection $\|w\|_\infty$ versus $1/\beta$ computed from the present 1-DOF model, with those from [8]–[10].

For the second cantilever microbeam geometry and for the stress-free clamped–clamped microbeam Fig. 9(a) and (b) depicts the deformed shape of the microbeams just prior to the pull-in voltage. They give an idea of the maximum deflection of the beam just before the pull-in voltage is reached.

The nondimensional pull-in parameter μ for different values of the beam width b, and with values of other parameters listed in Table II, computed with different MEMS models, is given in Figs. 10 and 11 for a cantilever and a clamped–clamped beam, respectively; the corresponding results for the maximum pull-in deflections are exhibited in Figs. 12 and 13. The curves are computed by using the simple 1-DOF model. For each beam, the nondimensional pull-in parameter μ increases monotonically with a decrease in the value of β from 2.0 to 0.2. From Figs. 12 and 13, it is clear that the nondimensional pull-in maximum deflection significantly changes with the width of the beam, and consistently differs from the values used in [11] for deriving empirical estimates of the pull-in voltage (0.45 for cantilever and 0.40 for clamped–clamped microbeams). Indeed, for the narrow microbeam with $\beta = 2$, the nondimensional pull-in maximum deflections are 0.56 and 0.66 for the cantilever and the clamped–clamped configurations, respectively.

VII. Conclusion

The main contributions of this study can be summarized as follows.

- The previously available models in the literature for studying electrically actuated microbeams do not give good estimates of the pull-in voltage for a narrow microbeam with width smaller than five times the thickness. The proper choices of the beam bending stiffness and the fringing field due to the finite width of the beam are generally not sufficient to accurately model narrow microbeams. The effect of the beam finite thickness should be considered in order to derive a consistent electromechanical model.
- The classical empirical formulas for computing the line to ground capacitance cannot be applied to narrow microbeams, since the aspect ratio of the microbeam cross section may exceed the typical aspect ratios of integrated circuits. Furthermore, when large deflections are considered, the gap size along the microbeam span may attain values larger than those encountered in typical electronic circuits. Therefore, empirical formulas are needed to properly describe the electrical capacitance of narrow microbeams. In this study, an empirical formula suitable for narrow microbeams is derived from least squares fit to values computed by the method of moments. Values obtained from this formula are compared with those from other formulas in the literature, and predictions from its use are shown to be valid for a narrow microbeam.
- A 1-DOF model that gives very good values of the pull-in voltage for narrow clamped–clamped, and cantilever beams has been proposed. It differs from the classical spring-mass model since the nonlinear stiffening due to the axial stress, charge redistribution and fringing fields

are taken into account. Moreover, the complete nonlinear behavior of the electrostatic force is retained and the pull-in voltage and deflections are treated as unknowns, i.e., the pull-in deflection is not empirically chosen as was done in [11]. It is shown that the pull-in deflections noticeably change with the aspect ratio of the beam cross section and cannot be determined *a priori*.

- The 1-DOF model results have been validated by comparing them with those obtained by solving the nonlinear 1-D boundary-value problem with the MLPG and the FE methods in conjunction with the DIPIE algorithm. Results from the MLPG, and the FE methods are virtually indistinguishable when the same number of nodes are used. The convergence rate of the DIPIE method does not vanish when the pull-in state is approached, and the number of iterations remains reasonable.
- The MLPG method represents an efficient alternative to the FE method for studying microbeams and estimating the pull-in parameters. In particular, the MLPG method is applicable to any microbeam geometry, and it does not require the use of a mesh on the MEMS domain. This alleviates mesh entanglement problems and remeshing difficulties that may arise when analyzing finite deformations of MEMS devices, and simplifies the generation of the numerical model since no interconnectivity rules among nodes are required.
- The computed pull-in voltage for a clamped–clamped and a cantilever microbeam is found to match well with that obtained from the solution of the 3-D problem with the commercial computer code ANSYS. The 3-D simulations are considerably more expensive than those for the proposed 1-D distributed model.

Appendix A
MoM

The potential ϕ for an arbitrary charge distribution per unit surface ρ_S is given by

$$\phi(y,z) = -\frac{1}{2\pi\epsilon_0\epsilon_r}\int_\Gamma \rho_S(\theta,\zeta)\ln\|(y,z)-(\theta,\zeta)\|d\Gamma + C_T \tag{27}$$

where $\|(y,z)-(\theta,\zeta)\| = \sqrt{(y-\theta)^2+(z-\zeta)^2}$ is the distance from the source point (θ,ζ) to the observation point (y,z), Γ is the overall boundary of the conductors, and C_T is a constant that may be neglected since it does not affect the charge distribution. Boundary conditions on the top and the bottom rectangle, say Γ_t and Γ_b, are $\phi = \bar{V}$ and $\phi = 0$, espectively. The boundary of each plate is subdivided into small elements,and the charge density ρ_{Si} is assumed to be constant in element i (piecewise constant basis functions). For convenience we use the same mesh of N_e elements for the two identical rectangles. By substituting the charge approximation into (27) and by imposing the boundary conditions at the geometric centers P_i of the $2N_e$ elements (collocation method), we obtain the following linear system of $2N_e$ equations in $2N_e$ unknowns collected in the vector $\boldsymbol{\rho}_S$:

$$\mathbf{L}\boldsymbol{\rho}_S = \mathbf{g}.$$

The generic entry of the coefficient matrix $\mathbf{L}$ is given by

$$\begin{aligned} i = j : L_{ii} =& \Delta\Gamma_i\left(\ln\left(\frac{\Delta\Gamma_i}{2}\right)-1\right)\\ i \neq j : L_{ij} =& -\Delta\Gamma_j\left(1-\ln\left\|P_j^{(2)}-P_i\right\|\right)\\ &-\left\|P_j^{(1)}-P_i\right\|\cos\beta_{ij}\ln\frac{\left\|P_j^{(2)}-P_i\right\|}{\left\|P_j^{(1)}-P_i\right\|}\\ &+\alpha_{ij}\left\|P_j^{(1)}-P_i\right\|\sin\beta_{ij}\end{aligned}$$

where $\Delta\Gamma_i$ is the length of the ith element, $P_j^{(1)}$ and $P_j^{(2)}$ are the extrema of the jth element, β_{ij} is the angle between the segments $P_j^{(1)}P_j^{(2)}$ and $P_j^{(1)}P_i$, and α_{ij} is the angle between the segments $P_iP_j^{(2)}$ and $P_iP_j^{(1)}$. We note that these angles can be computed by using Carnot's theorem. The element of the vector $\mathbf{g}$ equals $\bar{V}$ if it refers to an element of Γ_t and 0 if it refers to an element of Γ_b. From the knowledge of the distributed charge per unit surface area, the charge stored per unit line in each plate may be directly computed, and the capacitance per unit line estimated.

Appendix B
GMLS Approximation

The GMLS approximation [15] constructs a trial function on the entire domain from the knowledge of its values and of its first derivatives at some, suitably chosen, scattered points. Here,we briefly report a special case of the general formulation of [15] for the present problem.

Consider the function w having continuous first derivative on the domain $(0,1)$. The fictitious nodal values, and fictitious values of its first derivative at scattered points $N = \{x_1, x_2, \ldots, x_N\}$ in $[0,1]$ are collected into two N-vectors $\hat{\mathbf{w}} = [\hat{w}_1, \ldots, \hat{w}_N]^T$, and $\hat{\boldsymbol{\vartheta}} = [\hat{\vartheta}_1, \ldots, \hat{\vartheta}_N]^T$, respectively, where the superscript T indicates matrix transposition. The global approximation w^h on $(0,1)$ is defined by

$$w(x) \simeq w^h(x) = \mathbf{p}^T(x)\mathbf{a}(x), \quad x \in (0,1) \tag{28}$$

where

$$\mathbf{p}^T(x) = [1, x, x^2, \ldots, x^{m-1}] \tag{29}$$

is a complete monomial basis of degree $m-1$.

The m-vector $\mathbf{a}(x) = [a_1(x), \ldots, a_m(x)]^T$ is comprised of coefficients, which vary with the abscissa x and are to be determined. At each location $\bar{x}$ in $(0,1)$, these coefficients are determined by a local least square approximation of $w(x)$ on a small neighborhood $\Omega_{\bar{x}}$ of $\bar{x}$. The local approximation $w_{\bar{x}}(x)$ is defined by

$$w(x) \simeq w_{\bar{x}}(x) = \mathbf{p}^T(x)\mathbf{a}(\bar{x}), \quad x \in \Omega_{\bar{x}} \subset (0,1). \tag{30}$$

In the neighborhood $\Omega_{\bar{x}}$ of $\bar{x}$, the coefficients a_i are treated as unknown constants of a classical polynomial least square approximation. Therefore, they are determined by minimizing the

functional $J_{\bar{x}}$ representing the weighted discrete H^1 error norm and defined by

$$J_{\bar{x}}(\mathbf{a}) = \sum_{i=1}^{N} W_i(\bar{x})[w_{\bar{x}}(x_i) - \hat{w}_i]^2 + \sum_{i=1}^{N} W_i(\bar{x}) \left[w'_{\bar{x}}(x_i) - \hat{\vartheta}_i\right]^2. \quad (31)$$

Functions W_i are weight functions of node i and are characterized by the following properties: 1) they are continuous; 2) they equal one at $x = x_i$; and 3) they vanish when $x \notin [x_i - R, x_i + R]$ and are positive elsewhere. The parameter R measures semi-supports of the weight functions W_i.

The stationarity of $J_{\bar{x}}$ with respect to $\mathbf{a}$ yields

$$\mathbf{A}(\bar{x})\mathbf{a}(\bar{x}) = \mathbf{B}(\bar{x})\hat{\mathbf{s}} \quad (32)$$

where the $m \times m$ and the $m \times N$ matrices $\mathbf{A}$ and $\mathbf{B}$ and the $2N$ vector $\hat{\mathbf{s}}$ are defined by

$$\begin{aligned} \mathbf{A}(\bar{x}) &= \mathbf{P}^T\mathbf{W}(\bar{x})\mathbf{P} + (\mathbf{P}')^T\mathbf{W}(\bar{x})\mathbf{P}' \\ \mathbf{B}(\bar{x}) &= [\,\mathbf{P}^T \quad (\mathbf{P}')^T\,]\,\mathbf{W}(\bar{x}) \\ \hat{\mathbf{s}}^T &= \left[\,\hat{\mathbf{w}}^T \quad \hat{\boldsymbol{\vartheta}}^T\,\right]. \end{aligned} \quad (33)$$

Here, $\mathbf{P}$ and $\mathbf{P}'$ are the $N \times m$ matrices of real numbers defined by

$$\begin{aligned} \mathbf{P}^T &= [\,\mathbf{p}(x_1) \quad \ldots \quad \mathbf{p}(x_N)\,] \\ (\mathbf{P}')^T &= [\,\mathbf{p}'(x_1) \quad \ldots \quad \mathbf{p}'(x_N)\,] \end{aligned}$$

and $\mathbf{W}$ is the $N \times N$ diagonal matrix defined by

$$\mathbf{W}(\bar{x}) = \mathrm{Diag}\,[\,W_1(\bar{x}) \quad \ldots \quad W_N(\bar{x})\,].$$

Solving (32) for $\mathbf{a}(\bar{x})$ and substituting for $\mathbf{a}(\bar{x})$ in the global approximation (28), we get the GMLS approximation

$$w^h(x) = \boldsymbol{\psi}(x)^T\hat{\mathbf{s}} \quad (34)$$

where the basis functions $\boldsymbol{\psi}(x)$ are given by

$$\boldsymbol{\psi}(x)^T = \mathbf{p}(x)^T\mathbf{A}^{-1}(x)\,[\,\mathbf{P}^T \quad (\mathbf{P}')^T\,]\,\mathbf{W}(x). \quad (35)$$

The GMLS expansion (34) is well defined only if the matrix $\mathbf{A}$ in $(33)_1$ is nonsingular; see [15] for necessary conditions. We assume the same $C^{\alpha-1}(0,1)$ structure for all weight functions

$$W_i(x) = \begin{cases} \left(1 - \left(\frac{x-x_i}{R}\right)^2\right)^{\alpha}, & \text{if } x \in (x_i - R, x_i + R) \\ 0, & \text{if } x \notin (x_i - R, x_i + R). \end{cases} \quad (36)$$

ACKNOWLEDGMENT

The authors sincerely thank the anonymous reviewers for careful reading of the manuscript and for giving useful suggestions that have helped improve the work and its presentation. The authors would also like to thank A. Andres Pacheco Sanjuan for teaching them how to use ANSYS.

REFERENCES

[1] C. T. C. Nguyen, L. P. B. Katehi, and G. M. Rebeiz, "Micromachined devices for wireles communications," *Proc. IEEE*, vol. 86, no. 8, pp. 1756–1768, Aug. 1998.

[2] E. S. Hung and S. D. Senturia, "Extending the travel range of analog-tuned electrostatic actuators," *J. Microelectromech. Syst.*, vol. 8, no. 4, pp. 497–505, Dec. 1999.

[3] H. A. Tilmans and R. Legtenberg, "Electrostatically driven vacuum-encapsulated polysilicon resonators: Part II. Theory and performance," *Sens. Actuators A, Phys.*, vol. 45, no. 1, pp. 67–84, 1994.

[4] G. I. Taylor, "The coalescence of closely spaced drops when they are at different electric potentials," *Proc. Roy. Soc. A*, vol. 306, pp. 423–434, 1968.

[5] H. C. Nathanson, W. E. Newell, R. A. Wickstrom, and J. R. Davis, "The resonant gate transistor," *IEEE Trans. Electron Devices*, vol. ED-14, no. 3, pp. 117–133, Mar. 1967.

[6] L. D. Gabbay, J. E. Mehner, and S. D. Senturia, "Computer-aided generation of nonlinear reduced-order dynamic macromodels. I: Non-stress-stiffened case," *J. Microelectromech. Syst.*, vol. 9, no. 2, pp. 262–269, Jun. 2000.

[7] S. D. Senturia, R. M. Harris, B. P. Johnson, S. Kim, K. Nabors, M. A. Shulman, and J. K. White, "A computer-aided design system for microelectromechanical systems (MEMCAD)," *J. Microelectromech. Syst.*, vol. 1, no. 1, pp. 3–13, Feb. 1992.

[8] P. M. Osterberg and S. D. Senturia, "M-TEST: A test chip for MEMS material property measurement using electrostatically actuated test structures," *J. Microelectromech. Syst.*, vol. 6, no. 1, pp. 107–118, Mar. 1997.

[9] E. M. Abdel-Rahman, M. I. Younis, and A. H. Nayfeh, "Characterization of the mechanical behavior of an electrically actuated microbeam," *J. Micromech. Microeng.*, vol. 12, no. 6, pp. 759–766, 2002.

[10] J.-H. Kuang and C.-J. Chen, "Dynamic characteristics of shaped micro-actuators solved using the differential quadrature method," *J. Micromech. Microeng.*, vol. 14, no. 4, pp. 647–655, 2004.

[11] S. Pamidighantam, R. Puers, K. Baert, and H. A. C. Tilmans, "Pull-in voltage analysis of electrostatically actuated beam structures with fixed-fixed and fixed-free end conditions," *J. Micromech. Microeng.*, vol. 12, no. 4, pp. 458–464, 2002.

[12] M. I. Younis, E. M. Abdel-Rahman, and A. H. Nayfeh, "A reduced-order model for electrically actuated microbeam-based MEMS," *J. Microelectromech. Syst.*, vol. 12, no. 5, pp. 672–680, Oct. 2003.

[13] S. N. Atluri and T. Zhu, "A new meshless local petrov-galerkin (MLPG) approach in computational mechanics," *Computat. Mechan.*, vol. 22, no. 2, pp. 117–127, 1998.

[14] G. R. Liu, *Mesh Free Methods*. Boca Raton, FL: CRC, 2003.

[15] S. N. Atluri, J. Y. Cho, and H.-G. Kim, "Analysis of thin beams, using the meshless local Petrov-Galerkin method, with generalized moving least squares interpolations," *Computat. Mech.*, vol. 24, no. 5, pp. 334–347, 1999.

[16] I. S. Raju and D. R. Phillips, "Further developments in the MLPG method for beam problems," *CMES: Comput. Modeling Eng. Sci.*, vol. 4, no. 1, pp. 141–159, 2003.

[17] U. Andreaus, R. C. Batra, and M. Porfiri, "Vibrations of cracked beams using meshless local Petrov-Galerkin (MLPG) method," *CMES: Comput. Modeling Eng. Sci.*, vol. 9, no. 2, pp. 111–132, 2005.

[18] L. F. Qian, R. C. Batra, and L. M. Chen, "Elastostatic deformations of a thick plate by using a higher-order shear and normal deformable plate theory and two meshless local Petrov-Galerkin (MLPG) methods," *CMES: Comput. Modeling Eng. Sci.*, vol. 4, no. 1, pp. 161–176, 2003.

[19] ——, "Free and forced vibrations of thick rectangular plates by using higher-order shear and normal deformable plate theory and meshless Petrov-Galerkin (MLPG) method," *CMES: Comput. Modeling Eng. Sci.*, vol. 4, no. 5, pp. 519–534, 2003.

[20] ——, "Static and dynamic deformations of thick functionally graded elastic plate by using higher-order shear and normal deformable plate theory and meshless local Petrov-Galerkin method," *Composites: Part B*, vol. 35, no. 6-8, pp. 685–697, 2004.

[21] R. C. Batra, M. Porfiri, and D. Spinello, "Analysis of electrostatic MEMS using meshless local Petrov–Galerkin (MLPG) method," *Engi. Anal. Boundary Elem.*, 2006, 10.1016/j.engenebound.2006.04.008.

[22] L. D. Landau and E. M. Lifshitz, *Theory of Elasticity*. New York: Pergamon, 1986.
[23] O. Degani-Bochobza, D. Elata, and Y. Nemirovsky, "An efficient DIPIE algorithm for CAD of electrostatically actuated MEMS devices," *J. Microelectromech. Syst.*, vol. 11, no. 5, pp. 612—620, Oct. 2002.
[24] R. F. Harrington, *Field Computation by Moment Methods*. Piscataway, NJ: IEEE Press, 1993, pp. 229–229.
[25] D. Iesan, *Saint-Venant's Problem*. New York: Springer-Verlag, 1987.
[26] T. Mura and T. Koya, *Variational Methods in Mechanics*. New York: Oxford Univ. Press, 1992.
[27] E. Barke, "Line-to-ground capacitance calculation for VLSI: A comparison," *IEEE Trans. Comput.-Aided Des. Integr. Circuits Syst.*, vol. 7, no. 2, pp. 295–298, Feb. 1988.
[28] E. R. Collins, *Foundations for Microwave Engineering*, 2nd ed. New York: McGraw-Hill, 1992, pp. 130–153.
[29] H. B. Palmer, "Capacitance of a parallel-plate capacitor by the Schwartz-Christoffel transformation," *Trans. Amer. Inst. Elect. Eng.*, vol. 56, no. 3, pp. 363–366, 1937.
[30] N. V. D. Meijs and J. T. Fokkema, "VLSI circuit reconstruction from mask topology," *Integration*, vol. 2, no. 2, pp. 85–119, 1984.
[31] W. H. Press, B. P. Flannery, S. H. Teukolsky, and W. T. Vetterling, *Numerical Recipes*. New York: Cambridge Univ. Press, 1989.
[32] K.-J. Bathe, *Finite Element Procedures*. Englewood Cliffs, NJ: Prentice-Hall, 1996.
[33] Pull-in Voltage Analysis of Electrostatically-Actuated Beams Verifying Accuracy of Coventor Behavioral Models Coventor Inc. [Online]. Available: www.coventor.com
[34] R. J. Shapoorabadi and A. G. Kirk, "Comparison of three finite element models for analysis of MEMS micromirrors," in *Proc. SPIE Int. Conf. Appl. Photon. Technol., Photonics North*, 2004, vol. 5577, pp. 849–859.
[35] ANSYS Release 8.0 Documentation Ansys, Inc..

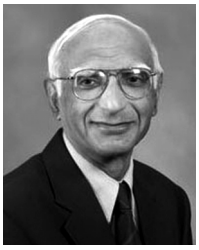

Romesh C. Batra received the B.Sc. degree in mechanical engineering from the Thapar College of Engineering (now called Thapar University), Patiala, India, in 1968, the M.A.Sc. degree in mechanical engineering from the University of Waterloo, Waterloo, ON, Canada, in 1969, and the Ph.D. degree in mechanics and materials science from the Johns Hopkins University, Baltimore, MD, in 1972.

He is the Clifton C. Garvin Professor of Engineering Science and Mechanics at Virginia Polytechnic Institute and State University, Blacksburg, VA. His research interests include smart materials/structures, ductile failure, penetration mechanics, computational mechanics, and functionally graded materials.

Prof. Batra is a Fellow of the American Society of Mechanical Engineers (ASME), the American Academy of Mechanics, the Society of Engineering Science, and the American Society of Engineering Education. He has been inducted into the Hopkins Society of Scholars and was the recipient of the Alexander von Humboldt Award in 1992 and the Reissner Medal from the International Society of Computational Engineering Science in 1996. He served as President of the Society of Engineering Science in 1996.

Maurizio Porfiri was born in Rome, Italy, in 1976. He received the M.Sc. and Ph.D. degrees in engineering mechanics from the Virginia Polytechnic Institute and State University, Blacksburg, the "Laurea" degree in electrical engineering (with honors) and the Ph.D. degree in theoretical and applied mechanics from the University of Rome "La Sapienza," Rome, Italy, in 2001 and 2005, respectively, and the Ph.D. degree in mechanics from the University of Toulon et du Var, Toulon, France in 2005.

He is currently an Assistant Professor in the Department of Mechanical, Aerospace and Manufacturing Engineering, Polytechnic University, Brooklyn, NY. His research interests include computational mechanics, mathematical control theory, mechatronics, microelectromechanical systems, robotics and vibrations.

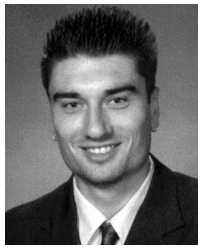

Davide Spinello was born in Latina, Italy, in 1977. He received the B.S. and "Laurea" (with honors) degrees in environmental engineering from the University of Rome "La Sapienza," Rome, Italy, in 2001 and 2005. He is currently working toward the Ph.D. degree in engineering mechanics at the Virginia Polytechnic Institute and State University, Blacksburg.

His research interest include computational mechanics and microelectromechanical systems. His doctoral dissertation defense is scheduled in August 2006.